ELSEVIER

Biochimica et Biophysica Acta 1329 (1997) 223–236

BIOCHIMICA ET BIOPHYSICA ACTA
BBA

Structural characterisation of the natural membrane-bound state of melittin: a fluorescence study of a dansylated analogue

Enrique Pérez-Payá [a], Jean Dufourcq [b], Lorenzo Braco [a], Concepción Abad [a,*]

[a] *Departament de Bioquímica i Biologia Molecular, Universitat de València, E-46100 Burjassot, València, Spain*
[b] *Centre de Recherche Paul Pascal, CNRS, F-33600 Pessac, France*

Received 18 February 1997; accepted 28 April 1997

Abstract

The binding of a dansylated analogue of melittin (DNC–melittin) to natural membranes is described. The cytolytic peptide from honey bee venom melittin was enzymatically labelled in its glutamine-25 with the fluorescent probe monodansylcadaverine using guinea pig liver transglutaminase. The labelled peptide was characterised functionally in cytolytic assays, and spectroscopically by circular dichroism and fluorescence. The behaviour of DNC–melittin was, in all respects, indistinguishable from that of the naturally occurring peptide. We used resonance energy transfer to measure the state of aggregation of melittin on the membrane plane in synthetic and natural lipid bilayers. When bound to erythrocyte ghost membranes, the extent of energy transfer was found to be equivalent to when bound to small unilamellar vesicles of phosphatidylcholine. Our results correlate best with a proposed model in which the initial interaction between melittin and the red blood cells could be merely electrostatic and the peptide remains in a low α-helical conformation. The next step would be a peptide stabilisation in the membrane in a monomeric α-helical conformation that would imply the collapse of the membrane structure and liberation of the cell contents. © 1997 Elsevier Science B.V.

Keywords: Dansyl labeling; Melittin; Fluorescence energy transfer; Lipid-protein interaction; Natural membrane

1. Introduction

Studies on the interactions between membranes and peptides are central to the knowledge of the insertion process of membrane proteins, the binding of hormones to membrane receptors and the action of antibiotic peptides and toxins. The general principles of the mechanism of interaction of surface-active peptides with membranes are understood, but the details necessary for a quantitative structure-activity and thermodynamic frameworks remain elusive.

One of the best studied surface-active peptides is melittin, the predominant peptide isolate from honey bee (*Apis mellifera*) venom. Melittin is a haemolytic peptide consisting of 26 amino acid residues, with strong amphipathic surface activity, and is known to adopt various conformations and aggregation states in different aqueous solutions [1–4]. At high peptide concentration or at high ionic strength, melittin self associates into a tetrameric structure [3,5,6]. The relationship between the tetrameric self assembly of melittin and its biological activity has been linked to the necessity to prevent peptide's hydrophobic

* Corresponding author. Fax: +34-6-3864635; E-mail: paya@uv.es

PII S0005-2736(97)00112-0

residues from being exposed to the sugar charges present in biological membranes [2].

The interaction of melittin with membranes is of particular interest because of the complex equilibrium predicted for the distribution of the amphipathic peptide between the aqueous phase, the membrane surface, whether or not the presence of membrane proteins affect the equilibrium and how a new melittin–phospholipid complex is generated after disruption of the membrane. In the presence of model membranes melittin adopts an amphipathic α-helical conformation such as might occur at cell surfaces [7]. But conflicting results have been reported on the state of aggregation of the helices on the membrane plane, that would be the bioactive conformation [8–12]. Studies using lipid vesicles and measuring fluorescence energy transfer between melittin as donor and a modified melittin as acceptor, indicate that melittin in membranes forms tetramers in a concentration and ionic strength-dependent manner [11,12]. In contrast, other groups found no evidence for aggregation in fluid membranes [8–10,13]. Although many additional questions can be raised concerning the disparity of the results such as membrane lipid composition used, in our view, the main point is that most of such studies deal with analogues where the lytic activity of the melittin analogues was significantly or drastically decreased or not checked.

The propensity of small-sized amphipathic peptides to interact with membrane proteins has been described. Thus, previous studies of the effect of melittin on the rotational diffusion of the bacteriorhodopsin in reconstituted Mys_2PtdCho vesicles, and band 3 protein in erythrocyte membranes [14–16], showed that the presence of melittin restricted protein rotational diffusion. Such an effect could be due to direct peptide–protein interactions [14,16], but also via lipid properties changes.

Despite an extensive study of the interaction of melittin with model membranes, quantitative binding of melittin to biological membranes has only scarcely been measured using radiolabelled peptide [17]. But no data account for the structural state of melittin after the cell lysis and contradictory conclusions can be found in the literature about the ability of melittin to solubilise membrane fragments [17–19], although such solubilisation of lipids can indeed occur with pure lipids bilayers [20].

In order to gain insight on the molecular mechanism of peptide–cell membrane interaction, it is required to incorporate extrinsic spectroscopic probes into the peptides. The binding steps can then be monitored by following changes in the signal of the probe. Environmentally sensitive extrinsic fluorescent probes are particularly well suited for this purpose because their excitation and emission wavelengths can be chosen to minimise interference from background signals in the biological samples. However, care must be taken to ensure that the modification does not alter the biological activity of the labelled peptide in order to confirm that the observations one makes using the labelled peptide, are totally valid for the behaviour of the native toxin acting on its cell target.

We have reported the incorporation of the fluorescent probe monodansylcadaverine (DNC) into melittin's Gln^{25} (analogue DNC–melittin) when catalysed by guinea-pig liver transglutaminase [21,22]. The work presented here describes the structural characterisation by means of fluorescence and circular dichroism (CD) spectroscopies of DNC–melittin under a variety of experimental conditions in order to confirm that the labelled peptide retains the properties of the native sequence.

The DNC–melittin analog described here, displays normal biological activity and provides qualitative and quantitative information about the binding to biological membranes, the role of the membrane proteins, and how a new peptide–phospholipid complex is stabilised when the cytolytic toxin acts on their target cells.

2. Materials and methods

2.1. Materials

Melittin (research grade) and monodansylcadaverine, *N*-(5-aminopentyl)-5-dimethylamino-1-naphthalene sulfonamide (DNC) were from Serva (Heidelberg, Germany). Guinea pig liver transglutaminase (TGase; *R*-glutaminyl-peptide:amine γ-glutamyltransferase, EC 2.3.2.12) was from Sigma (St. Louis, MO). Egg phosphatidylcholine (PtdCho), lysopalmitoylphosphatidylcholine (LysoPtdCho), brain phosphatidylserine (PtdSer) and dipalmitoylphospha-

tidylcholine ($Pam_2PtdCho$) were from Sigma (St Louis, MO).

2.2. TGase-mediated labelling of melittin by monodansylcadaverine

Melittin was labelled at its Gln^{25} using the standard procedure previously described [22]. Briefly, melittin (400 μg) was incubated at 37°C for 18 h with 5 μM TGase in 100 mM Mes–NaOH buffer (pH 6.5) containing 20 mM DTT, 40 mM $CaCl_2$ and 1.4 mM DNC (final volume 100 μl). The reaction was stopped by heating at 60°C for 5 min [23]. Purification of DNC–melittin was carried out by RP–HPLC on a Waters (Milford, MA) instrument equipped with a μBondapak C_{18} column. A linear gradient of acetonitrile and water containing 0.1% trifluoroacetic acid comprised the mobile phase. Details of the purification have been described elsewhere [21].

2.3. Haemolytic assay

The haemolytic activities of the peptides were determined by two different methods using human red blood cells (RBCs). The blood was collected in EDTA-containing tubes, maintained at 4°C, and used either the same or the following day. In the first method, the cells were washed three times with isotonic sucrose-phosphate buffer (300 mM sucrose, 10 mM sodium phosphate, pH 7.3). Washed cells were exposed to equal amounts of melittin or DNC–melittin, and the extent of haemolysis was monitored as a function of time by measuring the transmittance of 650 nm light through the erythrocyte suspensions as described by Weaver et al. [24]. In the second method, the cells were washed three times with isotonic Tris–buffer (20 mM Tris–HCl, 130 mM NaCl, 1 mM EDTA, pH 7.0) and resuspended in the same buffer. Increasing amounts of melittin and DNC–melittin were added from aliquots of concentrated stock solutions to the erythrocytes suspension (final concentration 2.7×10^7 cells ml^{-1}). Mixtures were incubated for 3 h at 37°C and centrifuged at $800 \times g$ for 10 min. Haemoglobin in the supernatant was estimated spectrophotometrically at 414 nm. Isotonic Tris–buffer and Triton X-100 1% controls were used to determine 0% and 100% haemolysis, respectively, using the same erythrocyte suspension described above.

2.4. Phospholipid vesicles

Unilamellar vesicles were prepared by sonication of phospholipid dispersions as already described [2]. Erythrocyte ghost membranes were prepared by the method of Hanahan and Ekholm [25] and the lipid content was calculated according to Sweeley and Dawson [26].

2.5. Fluorescence and anisotropy

Peptide concentrations for melittin and DNC–melittin solutions were determined by UV spectrophotometry using $\epsilon_{280} = 5570\ M^{-1}\ cm^{-1}$ for Trp [27] and $\epsilon_{330} = 4640\ M^{-1}\ cm^{-1}$ for the dansyl group [28]. Steady-state fluorescence measurements were carried out at 23°C on a Perkin–Elmer (Beaconsfield, UK) LS-5B spectrofluorimeter coupled to a Model 3700 data station using a 2.5 nm slit width. Unless otherwise stated, the buffer was 50 mM Mops–NaOH, 1 mM EDTA, pH 7.0. DNC–melittin excited at 280 nm, yields an emission from 300 to 550 nm, due to the single Trp^{19} amino acid and the fluorescence emission of the attached dansyl group due to resonance energy transfer (RET). Fluorescence emission spectra of the dansyl group was obtained by excitation at 330 nm. The spectra were corrected by comparison to a quinine sulphate standard. Always the possible weak fluorescence contribution due to the buffer and/or lipid solutions without peptides was used as baseline in all the experiments and subtracted. The wavelength shifts were estimated by changes of the wavelength of the mid-point at two-thirds the height of the spectral band. The relative variation of the fluorescence intensity was expressed by the ratio $\Delta I / I_0$ where I_0 is the intensity of the maximum fluorescence of the free peptides and ΔI is the change in fluorescence intensity upon binding to the phospholipid vesicles at the same wavelength.

Fluorescence excitation spectra were recorded from 250 to 400 nm with emission wavelength settled at 510 nm. The efficiency of energy transfer, *E*, was determined from the excitation spectrum using the energy acceptor method [29]. This method was chosen because it can be used even if the local environ-

ment of the donor is different in the presence of an acceptor. The transfer efficiency is given by

$$E = \left[G(\lambda_2)/G(\lambda_1) - \epsilon_A(\lambda_2)/\epsilon_A(\lambda_1)\right] \times \left[\epsilon_A(\lambda_1)/\epsilon_D(\lambda_2)\right] \quad (1)$$

were $G(\lambda)$ is the magnitude of the corrected excitation spectrum of the energy acceptor excited at wavelength λ. The extinction coefficients of the energy donor and acceptor at that wavelength are $\epsilon_D(\lambda)$ and $\epsilon_A(\lambda)$, respectively. G is measured at two wavelengths: At λ_1, where the donor has no absorption (i.e., 330 nm), and λ_2, where the extinction coefficient of the donor is large compared to that of the acceptor (i.e., 280 nm). For calculating the distances between two sites by energy transfer, the Förster energy transfer distance R_0, at which the efficiency of energy transfer between a donor–acceptor pair is 50%, has to be estimated. R_0 can be calculated from Eq. (2) [29],

$$R_0 = 9.79 \times 10^3 \left(\kappa^2 n^{-4} \Phi_D J_{DA}\right)^{1/6} \text{ (Å)} \quad (2)$$

where κ^2 is an orientation factor, n is the refractive index of the medium, Φ_D is the quantum yield of the donor in the absence of the acceptor, and J_{DA} is the spectral overlap integral, which is defined as in Eq. (3) [29],

$$J_{DA} = \int F_D(\lambda)\epsilon_A(\lambda)\lambda^4 d\lambda / \int F_D(\lambda)\mathrm{d}\lambda \text{ (cm}^3\text{ M}^{-1}\text{)} \quad (3)$$

where $F_D(\lambda)$ and $\epsilon_A(\lambda)$ are the donor fluorescence and acceptor extinction coefficient, respectively. Simpson's rule for integral approximation was used for summation of the integral at 1 nm intervals. We used $\Phi(\text{Trp},H_20) = 0.13$ [30], and the values reported by Vogel and Jähnig [12] for the quantum yield of Trp in melittin (0.23 in solution and 0.36 in phospholipid membranes) and a value of 1.4 for the refractive index of the medium [31]. The distance between donor and acceptor from the energy transfer efficiency and R_0 can be calculated from Eq. (4).

$$E = R_0^6/\left(R^6 + R_0^6\right) \quad (4)$$

Fluorescence anisotropy was measured in a Perkin Elmer LS-50 spectrofluorimeter, with excitation and emission slits of 3 and 5 nm, respectively. The reported values of anisotropy, r, were the average of a series of 10 to 20 acquisitions using an integration time of 10 s.

2.6. Circular dichroism measurements

All measurements were carried out at 23°C on a Jobin Yvon CD6 circular dichroism spectropolarimeter (CD-Longjumeau, France) calibrated with isoandrosterone. Unless otherwise stated, the buffer for CD assays was 2.5 mM Mops–NaOH, 1 mM EDTA, 21.5 mM NaCl, pH 7.0 in quartz cell of 0.05 cm path length. CD spectra were the average of five to seven scans, made at 0.2 nm intervals, always the same buffer and/or lipid solutions without peptides, used as baseline, were subtracted. Fractional helicities were calculated as $f_H = (([\theta]_{222} - [\theta]^0_{222})/[\theta]^{100}_{222})$, from the experimentally observed mean residue elipticity $[\theta]$ at 222 nm. $[\theta]_{222}$ values corresponding to 100% and 0% helix content were respectively $[\theta]^{100}_{222} = -28400$ deg cm^2 dmol^{-1} and $[\theta]^0_{222} = -2000$ deg cm^2 dmol^{-1} [24].

3. Results

3.1. Characterisation of DNC–melittin in solution

When the dansyl group attached at Gln^{25} in labelled melittin is selectively excited at 330 nm [22], an emission maximum is observed at 563 nm due to the fluorescence of the dansyl (Fig. 1A). When DNC–melittin is excited at 280 nm, two emission maxima are observed corresponding to the tryptophan fluorescence at short wavelengths ($\lambda_{max} = 352$ nm) and the label fluorescence at longer wavelengths ($\lambda_{max} = 563$ nm). At low ionic strength in buffer where melittin is well known to be monomeric [1,3,4], native melittin shows the same emission maximum at 352 nm (Fig. 1A). However, the fluorescence intensity of the tryptophan on the labelled peptide is decreased compared to native melittin. This quenching can be due to energy transfer from the Trp^{19} residue to the dansyl group.

It is well known that melittin can be induced into an α-helical conformation by increasing solution ionic strength, this conformational change is concomitant with a monomer-to-tetramer transition [1,3]. Tetrameric melittin is characterised by a blue shifted Trp emission at 334 nm, reflecting some shielding of the tryptophan residues from the solvent. When ionic strength is severely increased, the emission spectra of DNC–melittin changes as shown in Fig. 1A, the

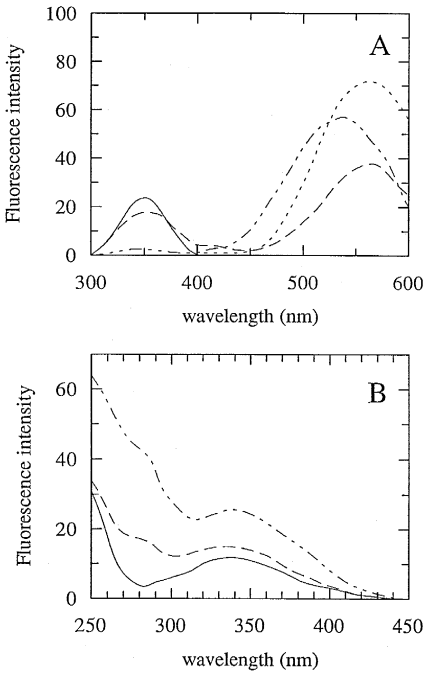

Fig. 1. Fluorescence emission (A) and excitation (B) spectra of melittin and DNC–melittin in buffer. The fluorescence spectra were recorded at a peptide concentration of 7 μM. 1:1 mixture of native melittin and free DNC (————) and DNC–melittin (— — ——) excitation wavelength 280 nm in (A) and observation wavelength 510 nm in (B); DNC–melittin (---) excitation wavelength 330 nm and DNC–melittin in the presence of 1 M NaCl (———— - -) excitation wavelength 280 nm in (A) and observation wavelength 510 nm in (B).

tryptophan fluorescence is quenched at the expense of a concomitant increase in the fluorescence of the dansyl label. In the aggregated form of DNC–melittin, the tryptophan residues should be closer to the dansyl group than in the monomer, and they contribute to the fluorescence of the probe because of energy transfer. To better define what is the process involved, we analysed the excitation spectra of DNC–melittin which are shown in Fig. 1B. When the emission is settled at 510 nm the peak centred at 280 nm corresponds to the absorption of the Trp^{19}. Its intensity was lowest in the absence of NaCl, where the peptide is monomeric. Increasing the NaCl concentration (which induces tetramerisation) leads to an increase of the intensity at 280 nm until a maximum is reached at salt concentration of about 1 M NaCl. The excitation spectrum of an equimolar mixture of free DNC and native melittin (Fig. 1B) shows a minimal contribution at 280 nm due to the dansyl. Moreover, this spectrum does not reveal any energy transfer between unlabelled peptide and free DNC. From the corrected energy transfer efficiency (E), the distance between the donor (Trp) and acceptor (dansyl) can be determined using Eq. (4) (cf. Section 2). This equation requires the calculation of J_{DA} and R_0. We obtained $J_{DA} = 3.33 \times 10^{-15}$ cm^3 M^{-1} and $R_0 = 20.1$ Å in salt free buffer and $J_{DA} = 4.02 \times 10^{-15}$ cm^3 M^{-1} and $R_0 = 22.8$ Å in the presence of 1 M NaCl. These R_0 values are within the ranges of those reported in the literature [30]. Using these values, the intramolecular distance (R) between Trp^{19} and the dansyl group at Gln^{25} was estimated to be 19.3 Å for monomeric DNC–melittin and 15.8 Å for the structured aggregate.

As mentioned above excitation at 330 nm allows to monitor the fluorescence emission of dansyl in DNC–melittin. The fluorescence parameters of the probe change with peptide self-association; the maximum of emission moves to 545 nm at high salt concentration (1 M NaCl) from its position at 563 nm in salt free buffer which indicates that the dansyl group of DNC–melittin is in a less polar environment. In contrast to DNC–melittin, the emission maximum of free DNC was insensitive to the presence of salt (Fig. 2A).

The anisotropy of the tryptophan fluorescence is also a valuable tool to follow the self association of melittin in solution [32]. We determined the steady-state anisotropies of both, tryptophan and dansyl in DNC–melittin. In salt free buffer, the anisotropy value for tryptophan in DNC–melittin ($r = 0.027 \pm 0.001$) was slightly higher than for the native peptide ($r = 0.021 \pm 0.003$). For the two peptides, the tryptophan anisotropy increases in a similar extent when the NaCl concentration was increased as a consequence of peptide self-association (Fig. 2B). The anisotropy of the dansyl label in the modified peptide also increases upon salt addition up to a plateau value for NaCl > 1 M. As an internal control free DNC anisotropy proved to be insensitive to changes in salt concentration (Fig. 2B).

The α-helical content of DNC–melittin and melittin was estimated by CD spectroscopy. As shown in Fig. 2C the fractional helix content (f_H) increases in a very similar way for both peptides upon titration with NaCl.

Table 1 summarises some characteristic parameters obtained for melittin and DNC–melittin in buffer, 1 M NaCl and methanol. All the above presented data show that the dansyl probe linked to melittin does not alter the salt-induced self association of the peptide, nor the solvent polarity effect. In fact, the relative changes observed in the position of the fluorescence emission maximum, the increases in anisotropy (for Trp^{19} and dansyl group) and in molar elipticity occur at rather similar NaCl concentration, the half reaction concentration being weaker for DNC–melittin, i.e., DNC has a weak promoting effect towards oligomerization.

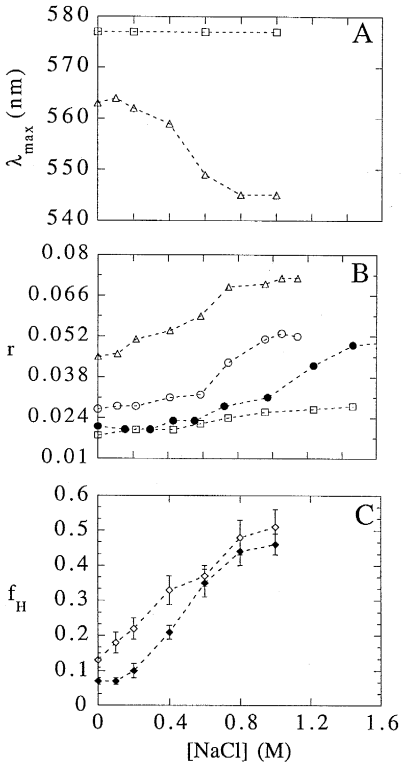

Fig. 2. Conformational behaviour of melittin and DNC–melittin at different ionic strengths. (A) Fluorescence emission maximum wavelength of the dansyl group upon excitation at 330 nm. (B) Fluorescence anisotropy with the excitation and emission monochromatorators settle at 280 and 340 nm, for Trp^{19} and 330 and 510 nm for the dansyl group, respectively. The fluorescence data were acquired at a peptide concentration of 7 μM. (□) free DNC; (Δ) dansyl group in DNC–melittin; (●) Trp^{19} of melittin or (○) DNC–melittin. (C) Fractional ellipticities (f_H) calculated as described in Section 2 for melittin (♦) and DNC–melittin (◇). Peptide concentration 30 μM.

Table 1
Structural parameters of melittin and DNC–melittin in solution [a]

	Buffer	NaCl 1 M	Methanol
Melittin			
f_H	0.07	0.46	0.72
λ_{max} (Trp^{19}) (nm)	352	345	342
r_{Trp}	0.021	0.039	nd
DNC–melittin			
f_H	0.13	0.53	0.78
λ_{max} (Trp^{19}) (nm)	352	350	342
λ_{max} (dansyl) (nm)	563	545	538
r_{Trp}	0.027	0.053	nd
r_{dansyl}	0.045	0.072	nd
E(%)	55	90	72
R_0 (Å)	20.1	22.8	23.6
R (Å)	19.3	15.8	20.2
free DNC			
λ_{max} (dansyl) (nm)	577	577	538
r_{dansyl}	0.018	0.028	nd

[a] f_H: fractional helicities, λ_{max}: fluorescence emission maximum; r: fluorescence anisotropy; E(%): energy transfer efficiency; R_0: Förster energy transfer distance; R: distance between donor and acceptor.
nd: not determined.

3.2. Binding of DNC–melittin to lipids

In order to evaluate the binding affinity of melittin and DNC–melittin to phospholipid vesicles, CD and fluorescence spectroscopy were used in combination. Fig. 3 shows the conformational changes of the binding of DNC–melittin to PtdCho small unilamellar vesicles (SUVs). Upon binding to lipids, its helical structure increases up to plateau values at $R_i > 100$. Like melittin itself, DNC–melittin showed a high f_H value which suggests that in the vesicle-bound state the peptides have similar helical conformation. Thus, the ability to be induced in an α-helical conformation is an intrinsic property dictated by the peptide sequence and it is not modified by the presence of the attached dansyl group.

The fluorescence of the Trp and dansyl groups in DNC–melittin is also sensitive to vesicles binding. Fig. 3B–C show that the maximum emission is al-

ways blue-shifted, by 30 nm for the attached-dansyl group and about 17 nm for Trp. The binding curves are very similar and monophasic which excludes a simple partition process to take place and they reach a plateau at the same phospholipid–peptide ratios (R_i = [phospholipid]/[peptide]). As a control, the binding of free DNC to PtdCho vesicles was also studied (Fig. 3B), but in this case the soft binding curve obtained represents a simple partition process of DNC between the aqueous and lipid phases with a partition coefficient $K_p = 2600$.

Melittin strongly binds to lysoPtdCho micelles and to negatively charged phospholipid membranes [20,32]. Fig. 4A shows the shifts in the maximum of

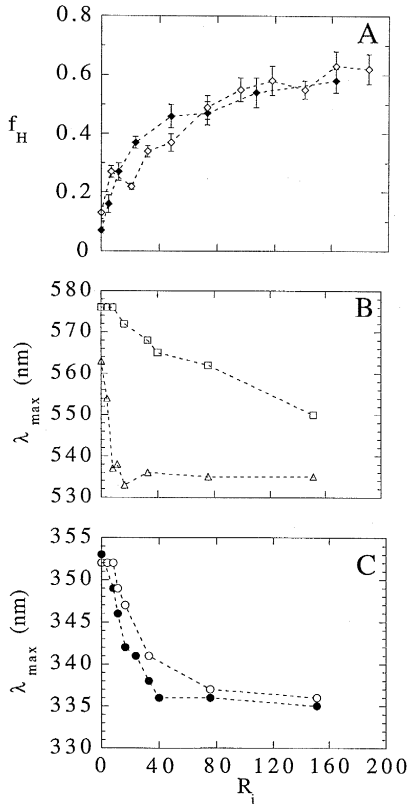

Fig. 3. Conformational behaviour of melittin and DNC–melittin in the presence of PtdCho SUVs. (A) fractional ellipticities (f_H) calculated as described in Section 2 for melittin (♦) and DNC–melittin (◇). (B) Fluorescence emission maximum wavelength of the dansyl group upon excitation at 330 nm in DNC–melittin (△) and in free DNC (□). (C) Fluorescence emission maximum wavelength of Trp[19] upon excitation at 280 nm in melittin (●) and DNC–melittin (○). The peptide concentration was 30 μM in the CD experiments and 7 μM in the fluorescence experiments. R_i is the molar phospholipid–peptide ratio.

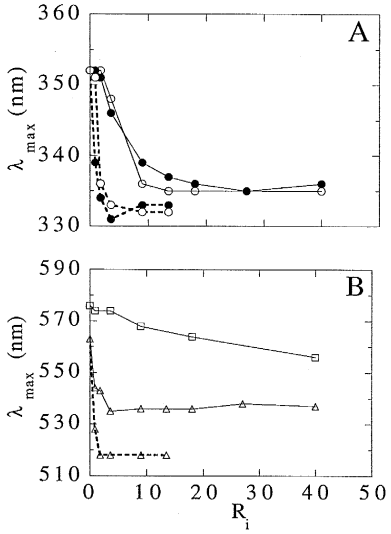

Fig. 4. Binding affinity curves of melittin and DNC–melittin to lysoPtdCho micelles (solid line) and PtdSer SUVs (dashed line). (A) Fluorescence emission maximum wavelength of Trp[19] upon excitation at 280 nm in melittin (●) and DNC–melittin (○). (B) Fluorescence emission maximum wavelength of the dansyl group upon excitation at 330 nm in DNC–melittin (△) and in free DNC (□).

Trp fluorescence emission of native and labelled melittin upon interaction with lysoPtdCho micelles and PtdSer SUVs. At saturation, for R_i ratios higher than 20, we obtained $\lambda_{max} = 335$ nm ($\Delta\lambda = 17$ nm) with the micelles (same value that we obtained when binding to PtdCho vesicles) and $\lambda_{max} = 331$ nm ($\Delta\lambda = 21$ nm) with the negatively charged vesicles. It seems likely that the tryptophan environment for the bound peptide is not exactly the same in these two different lipid systems as has been previously reported by Batenburg et al. [33]. In addition, the dansyl group in DNC–melittin, shows a blue shift $\Delta\lambda = 26$ nm when bound to lysoPtdCho micelles and $\Delta\lambda = 45$ nm when bound to PtdSer vesicles (Fig. 4B). This documents the occurrence of different polarity environments for the C-terminal segment of melittin when bound to zwitterionic or anionic phospholipids. This interpretation is similar to that reported earlier from surface pressure measurements in lipid monolayers [34].

The analysis of membrane-induced blue-shifts shows that the spectral properties of Trp[19] of melittin and DNC–melittin are similar, suggesting a similar position of the Trp residue in the bilayer for both

peptides. Independent information about the location of the Trp in the bound-peptide state, can be obtained from its accessibility towards quenchers. The fluorophore is almost completely shielded from the aqueous quencher I^- when the peptides are bound to PtdCho SUVs (data not shown). The quenching constants were estimated to be about 1 ± 0.2 M^{-1} for melittin and DNC–melittin. In contrast, for the peptides in solution the quenching constants were 13.1 M^{-1} for melittin and 9.2 M^{-1} for DNC–melittin, which indicates that in solution the Trp of DNC–melittin is partially shielded from the quencher because of the presence of the dansyl group. Very similar changes in accessibility of Trp are observed when using acrylamide as quencher. The quenching constants in the bound state are identical for melittin and DNC–melittin and about ten-fold decreased as compared to the peptides in solution (data not shown). We can conclude that the tryptophan residue in both, melittin and DNC–melittin, is probably at the same depth when binding to PtdCho SUVs, based on the similar quenching constants obtained for both peptides using an aqueous quencher (I^-) and a quencher with known ability to penetrate phospholipid bilayers (acrylamide, Refs. [33,35]).

3.3. Lytic activity and binding of DNC–melittin to ghost red blood cell membranes

The cytolytic assays using two different methods demonstrate that DNC–melittin and melittin have similar lytic activity. The efficacy of the peptides to lyse human erythrocytes was first assessed by monitoring the light scattering of human erythrocytes, as previously described [24]. We obtained that the relative rates of haemolysis were 7.1 and 3.1 min^{-1} μM^{-1} for the native and the labelled peptide, respectively. In addition, we analysed the haemolytic activity of both peptides using several peptide concentrations and measuring the haemoglobin release. The resulting 'Lytic Dose' necessary to lyse 50% of the cells (LD_{50}) were: $LD_{50} = 0.16$ μM for melittin and $LD_{50} = 0.23$ μM for DNC–melittin. These results could be related with previous studies on synthetic analogues of melittin which indicate that modifications of Gln^{25} do not involve substantial reduction of activity [36–38].

The above reported data show that the presence of the dansyl group in melittin does not impair the solution, nor the lipid binding properties, nor the biological activity of the native peptide. Moreover, since we have demonstrated that the dansyl group is more sensitive to membrane polarity changes than the melittin's intrinsic tryptophan, we conclude that DNC–melittin is a good analogue to study peptide–lipid interactions in more complex systems, i.e., using ghost or intact red blood cells.

The fluorescence emission spectra of DNC–melittin ($\lambda_{exc} = 330$ nm) are sensitive to the addition of ghost red blood cell membranes at different concentration ratios (Fig. 5A). The dansyl fluorescence pa-

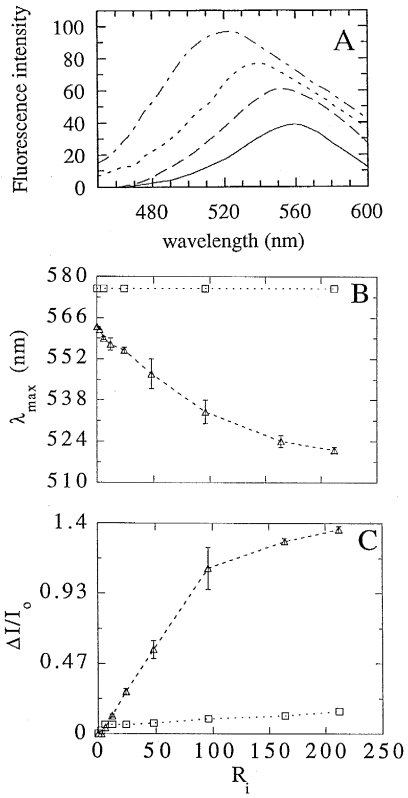

Fig. 5. Binding of DNC–melittin to ghost red blood cell membranes. (A) Fluorescence emission spectra ($\lambda_{exc} = 330$ nm) recorded at different phospholipid/peptide ratios, R_i. (————) $R_i = 0$; (—— ——) $R_i = 40$; (- -) $R_i = 80$; (———— –) $R_i = 200$. (B) Fluorescence emission maximum wavelength of the dansyl group upon excitation at 330 nm in DNC–melittin (△) and in free DNC (□). (C) Relative variation of the fluorescence intensity ($\lambda_{exc} = 330$ nm) expressed as the ratio $\Delta I/I_0$ where I_0 is the intensity at 510 nm and ΔI is the change in fluorescence intensity upon binding to the ghost red blood cell membranes at the same wavelength.

rameters change upon increasing R_i, indicating a progressive burying of the probe in the membrane as seen in Fig. 5B–C. Although the overall shape of the binding curve is rather smooth, similarly to that obtained when the peptide interacts with PtdCho vesicles, the blue-shift observed, $\Delta\lambda = 42$ nm, is similar to that of obtained in the presence of PtdSer vesicles (Fig. 4B). This large blue-shift for the dansyl group of DNC–melittin when binding to the ghost red blood cell membranes, indicates that the peptide is inserted in an average environment that is much more hydrophobic than when bound to zwitterionic PtdCho vesicles.

3.4. Quantitative analysis of the binding of DNC–melittin to membranes

The binding of melittin and DNC–melittin to PtdCho SUVs and of DNC–melittin to ghost red blood cell membranes was quantitatively analysed using the two-state model, assuming that the peptide is either free in solution or bound to the lipids in an unique state. This model allows the estimation of the dissociation equilibrium constant, K_d; and the number of lipid molecules needed to define a peptide binding site, N. Experimentally, the fluorescence intensity increases in the presence of lipids and allows to estimate the characteristic change in intensity for peptides totally bound from a double-reciprocal plot of $\Delta I / I_0$ vs. R_i. This defines the fraction of peptide bound (α) vs. R_i (Fig. 6). One can notice that the α values obtained for DNC–melittin with PtdCho differ significantly according to whether changes of the dansyl or the Trp fluorophore are monitored. On the other hand, the change of α obtained from the dansyl fluorescence in the presence of either SUV or ghost membranes is different. Fig. 6 also shows that good fits for all the experimental data can be obtained by using the proposed model. The dissociation constants and the N values found were: (a) From Trp fluorescence data analysis of melittin and DNC–melittin in the presence of PtdCho SUVs, $K_d = 1.2 \times 10^{-6}$ M, $N = 14$. (b) From dansyl fluorescence data analysis of DNC–melittin in PtdCho SUVs, $K_d = 1.0 \times 10^{-6}$ M, $N = 7$. (c) From dansyl fluorescence data analysis of DNC–melittin in the presence of ghost red blood cell membranes, $K_d = 0.7 \times 10^{-6}$ M, $N = 53$. The dissociation constant obtained are in good agreement with the previously reported, $K_d = 1.0 \times 10^{-6}$ M [39] obtained from sedimentation experiments with red blood cell membranes pre-treated with melittin.

3.5. Structure of the membrane bound state of DNC–melittin as documented by RET

Energy transfer efficiencies (E) obtained from the excitation spectra were measured to determine the degree of melittin aggregation in the presence of model membranes and in the presence of ghost red blood cell membranes. When using model membranes and regardless of the nature of the lipid system studied, the dependence of E vs. R_i shows a bimodal curve shape (Fig. 7A). Upon addition of small amounts of SUVs in the liquid crystalline state (PtdCho at 24°C or Pam_2PtdCho at 50°C) to monomeric DNC–melittin, initially the E values slightly increase, and in a second step at $R_i > 20$–40 a gradual decrease in E was observed. At $R_i = 150$, the RET efficiency of the DNC–melittin–PtdCho complex measured is identical to the value for free monomeric DNC–melittin (Fig. 7A). A biphasic behaviour was also observed when using other lipids. Small amounts of lysoPtdCho micelles or PtdSer SUVs, i.e., at R_i ratios from 5 to 10, increase the percentages of energy transfer up to as higher as 90%, then the percentage of energy transfer decreases as R_i increases. If we consider that the observed

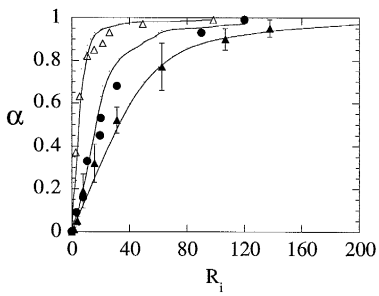

Fig. 6. Binding isotherms of DNC–melittin to membranes. The binding isotherms are derived from plots of fluorescence increase of Trp[19] (●) of melittin or DNC–melittin, and DNC (△) of DNC–melittin upon titration with PtdCho SUVs, and from fluorescence increase of the DNC group of DNC–melittin upon titration with ghost red blood cell membranes (▲). α is the molar fraction of peptide bound. The lines are the fits to the experimental data obtained when using the two states model (see text).

decrease in energy transfer is due to a dilution of bound peptides in the membrane plane, then addition of native melittin (energy donor) to a preformed lipid–DNC–melittin complex at high R_i, should increase the fluorescence intensity at 280 nm in the excitation spectra. In fact, we obtained undistinguishable excitation spectra when using $R_i = 10 =$ [lysoPtdCho]/[DNC–melittin] or using $R_i = 10 =$ [lysoPtdCho]/[[DNC–melittin] + [melittin]], obtained by addition of native melittin to a preformed lysoPtdCho–DNC–melittin complex at $R_i = 75$.

To document whether the initial conformational state of melittin may affect its degree of aggregation when bound to lipid bilayers, we examined the excitation spectra of DNC–melittin when bound to PtdCho SUVs (at $R_i = 150$) at different ionic strengths. The values of RET efficiency were then compared to that of the peptide alone. Fig. 7B shows that in the bound state the RET efficiency is significantly lower than the value obtained at the same ionic strength in solution. These results suggest that at high lipid concentration and ionic strength melittin is not in the

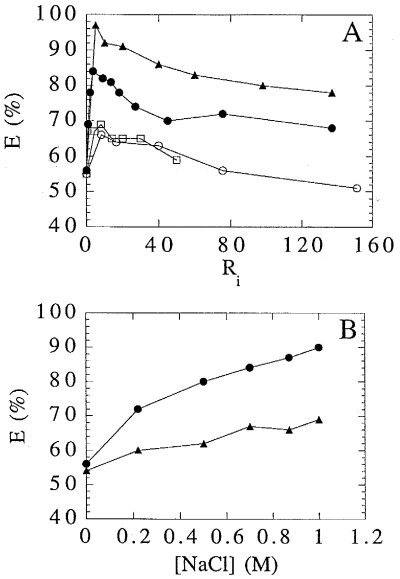

Fig. 7. Energy transfer efficiencies (E) between Trp^{19} and the dansyl group of DNC–melittin in the presence of phospholipid vesicles. The E values were measured as described in Section 2 from the fluorescence excitation spectra of (A) 7 μM DNC–melittin upon titration with PtdCho (○),Pam_2PtdCho (□), lysoPtdCho (●) and PtdSer (▲) and (B) DNC–melittin in the presence (▲) or absence (●) of PtdCho ($R_i = 150$) at different concentrations of NaCl.

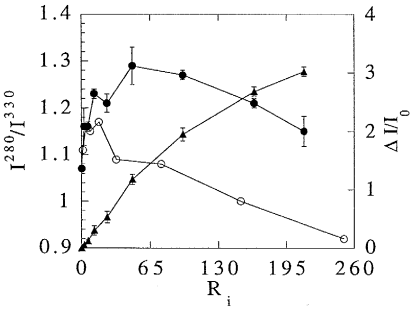

Fig. 8. Effects of the binding of DNC–melittin to ghost red blood cell membranes on the fluorescence parameters. Normalised increase of the fluorescence emission at 340 nm ($\lambda_{exc} = 280$ nm) of a 7 μM solution of DNC–melittin in the presence of ghost red blood cell membranes at different R_i (▲) and variation of the ratio I^{280}/I^{330} (ratio of fluorescence intensity in the excitation spectrum at 280 and 330 nm upon observation at 510 nm, (●) in the same experimental conditions. The variation of the ratio I^{280}/I^{330} in the presence of PtdCho at different R_i (○) that was used for the calculation of the E values in Fig. 7 has been included as reference.

'soluble tetramer-like' form in the phospholipid bilayer, though at such high ionic strength the peptide is self-associated in solution.

In an attempt to determine whether melittin is predominantly interacting with phospholipids or whether it can be in the neighbourhood of intrinsic proteins present on the red blood cell membrane, we measured the RET process upon addition of ghost red blood cell membranes to monomeric DNC–melittin. In this experiment, one has to keep in mind that by increasing ghost membrane concentration, the total concentration of protein increases. Thus, as expected the addition of ghost membranes resulted in a linear increase in the fluorescence emission at 340 nm ($\lambda_{exc} = 280$ nm) as shown in Fig. 8. Concomitantly, the intensity at 280 nm of the excitation spectra, upon observation at 510 nm, did not increase continuously as it should occur if energy was transferred between intrinsic membrane proteins and the dansyl probe of DNC–melittin. Since it is not possible to get the actual Trp concentration of donors in the ghosts membranes, it is not possible to estimate RET efficiency properly. However, as representative of transfer, we used the fluorescence ratio I^{280}/I^{330} from the excitation spectra with $\lambda_{obs} = 510$ nm. As shown on Fig. 8, the binding curve shape obtained is similar to those previously shown when measuring the RET

Table 2
Structural parameters of melittin and DNC–melittin when interacting with lipids and cell membrane [a]

	Melittin	DNC–melittin		
LD_{50} (μM)	0.16 PtdCho	0.23 PtdCho	PtdSer	Ghosts
f_H	0.65	0.65	nd	nd
$\Delta\lambda_{max}$ (dansyl) (nm)	–	26	45	42
E(%) at $R_i = 150$	–	50	80	≈ 80 [b]

[a] f_H: fractional helicities, λ_{max}: fluorescence emission maximum; E(%): energy transfer efficiency; K_d: dissociation equilibrium constant.
nd: not determined.
[b] The value was estimated from the comparison of the ratio I^{280}/I^{330} from the fluorescence excitation spectra of DNC–melittin in the presence of PtdCho and in the presence of ghost red blood cells.

on DNC–melittin when interacting with zwitterionic phospholipid membranes (Fig. 7A). This is consistent with the idea that melittin does not interact with the intrinsic red cell membrane proteins in an appreciable extent under the conditions used in our spectroscopic studies. Table 2 summarises some characteristic parameters obtained for melittin and DNC–melittin in the lipid–bound state.

Another possibility offered by DNC–melittin is to look at its fluorescence (emission and excitation spectra) after the lysis of intact red blood cells. A suspension of 2.7×10^7 rbc ml^{-1} was incubated 3 h at 37°C in the presence of 2 μM of DNC–melittin as usual for lysis experiment. This led to more than 90% haemolysis as determined using the procedure described in Section 2. Upon excitation of the dansyl fluorophore at 330 nm, the fluorescence emission spectrum obtained in the supernatant after the sample being centrifuged at $800 \times g$ for 10 min, shows a maximum at around 512 nm. This proves that some DNC–melittin is not pelleted with the ghosts and that the dansyl group is in an environment similar to that of previously obtained in the presence of the ghost red blood cell membranes, i.e., it corresponds to melittin bound to lipids and not to unreacted free DNC–melittin. Furthermore, the excitation spectrum does not show significant increase at 280 nm (data not shown). This tends to suggest the possibility of peptide–phospholipid complex formation after melittin–induced red blood cells lysis. Because of its spectroscopic characteristics, such a complex could be mainly constituted by negatively charged phospholipids. If one envisions that some intrinsic membrane proteins are present in this complex, then they are not in close contact with the C-terminal of melittin because no energy transfer between intrinsic membrane protein tryptophan residues and dansyl group could be detected.

4. Discussion

The DNC–melittin analogue used herein has full biological activity and it behaves similarly to native melittin in solution and in its interaction with lipids. Furthermore, DNC–melittin has provided new information on the mechanism of interaction of cytolytic toxins with model and natural membranes.

Fluorescence and CD spectroscopies showed that in low ionic strength buffer melittin and DNC–melittin are essentially unstructured. The well established monomer-to-tetramer conformational change of melittin in aqueous solution is also found for DNC–melittin: As the medium ionic strength increases the peptide self-associates and adopts an α-helical conformation with a concomitant hydrophobic burying of Trp^{19} and dansyl groups. The RET efficiency between Trp^{19} and the dansyl allows to calculate a distance of $R = 19.3$ Å for the monomeric peptide, rather similar to that found in the more structured monomer in MeOH, $R = 20.2$ Å (Table 1). In the tetrameric aggregate, the average distance between the two fluorophores is decreased down to 15.8 Å which accounts for intermolecular RET contributions. This general behaviour agrees with the literature data [8,9,11] and with the tetrameric structure data from X-ray crystallography [5,6].

In the presence of phospholipid model membranes (PtdCho and PtdSer SUVs, and lysoPtdCho micelles), the native and labelled peptides showed the ability to be folded into an α-helical conformation. In addition, when followed by tryptophan fluorescence changes, the binding to model membranes looked very similar for both peptides. Furthermore, the use of the dansyl fluorescence allows to differentiate the bound states of the peptide in a quite more accurate manner since the emission wavelength varies by ca. 20 nm when

bound to PtdSer compared to PtdCho, while under the best conditions only a 4 to 5 nm shift can be hardly detected by tryptophan fluorescence. The deeper burying of the dansyl group when melittin is bound to PtdSer agrees with ion pairing formation between the positively charged C-terminal fragment of the peptide and the polar head of negatively charged phospholipids. Moreover, the presence of two different fluorophores in the same peptide molecule shows that the binding process is not a simple one since the binding isotherms obtained following the two fluorophores are quantitatively different (Fig. 3A–B, Fig. 6). The binding dissociation constants are rather similar but there is a two-fold change in the minimum number of lipids required to define a peptide binding site at the interface. The values correspond to an occupied surface of about 400 Å^2 as seen for the dansyl, or about 1000 Å^2 as seen for the Trp. Such values are in the range expected for the lipid-bound melittin state [6,40]. It has been postulated that when melittin seeks to interact with phospholipid membranes there is an initial electrostatic interaction involving the C-terminal fragment of the peptide [41]. The presence of the dansyl group in this fragment could be used to report that polarity changes had occurred that affect this C-terminal fragment while at exactly the same phospholipid to peptide ratio the Trp^{19} residue is still located in an 'aqueous-like' environment and CD spectroscopy indicates that the peptide remains in a low α-helical conformation ($f_H = 0.27$, Fig. 3A). Afterwards, hydrophobic interactions take place which induce the stabilization of a more defined α-helical structure ($f_H = 0.65$, Fig. 3A) that implies the burying of the tryptophan residue in the bilayer. Indeed according to the lipid to peptide ratio the position of the peptide could change: It could be with a low α-helical content and absorbed onto the surface or still flat but more structured in an α-helix and penetrating the phospholipid bilayer. Similar conclusions have been reported for the conformational changes of melittin upon insertion into phospholipid membranes [42,43], thus for melittin molecules undergoing the initial adsorption stage the percentage of α-helix estimated was 30% [43] while higher values have been reported for melittin inserted in phospholipid bilayers [2,38,43]

Most of the characteristics hold when direct interaction of DNC–melittin with cell membranes is followed. The dansyl fluorescence changes can be fitted quantitatively and yield a K_d value in the micromolar range in agreement with that obtained for radiolabelled toxin [17]; they also yield a significantly large number of lipids required to define a peptide binding site, equivalent to seven times that obtained for pure lipid model membranes. One interpretation is that the presence of membrane proteins could make sets of lipids unavailable to the toxin, although it could also be due to preferential binding to negatively charged lipids which indeed represent a lower amount compared to total lipids. In fact the emission maximum for DNC–melittin when bound to ghost red blood cells is at 521 ± 1 nm, which is quite similar to 517 ± 1 nm obtained when the peptide is bound to pure PtdSer. However, when bound to zwitterionic lipids, such as PtdCho or lysoPtdCho, the maximum remains at higher wavelength, namely $\lambda = 537$ nm. These findings are similar to those observed with a new synthetic series of dansylated highly haemolytic peptides [44]. If one considers the well known solvatochromic changes for the dansyl group according to the bulk dielectric constant of the medium (ϵ), then the equivalent ϵ values obtained are $\epsilon = 25$ for the zwitterionic membrane and $\epsilon = 8$ for the negatively charged and natural membranes [45]. In conclusion, one can propose that the dansyl group of DNC–melittin bound to erythrocyte membranes remains in the bilayer nearby the glycerol backbone, but in a more dehydrated state when the peptide is bound to PtdSer due to electrostatic ion pairing. This reinforce previous similar proposals on the arrangement of melittin in model lipid membranes but it is the first time that it is observed for natural membranes.

Dansyl labelling allowed also to settle transfer experiments which can document about the peptide structures in different conditions. Indeed there is an internal transfer between the two probes in the peptide as shown in Figs. 7 and 8. In buffer and pure MeOH, the distances calculated are coherent for what we know of the secondary structure. The point we would like to emphasize is that in the presence of lipids at very low R_i values (ca. $R_i = 10$), where neither significant secondary structure nor local Trp^{19} environment changes could be detected (see Fig. 3), we obtained the maximal energy transfer that could be due to intermolecular neighbourhood of donors

and acceptors (Fig. 7). When the R_i values are increased and the lipids recover their normal vesicular structure [20] the transfer smoothly decreased, that could be related with a dilution of peptides on the membrane plane. This documents a dynamic equilibrium and not a stabilisation of aggregated melittin, which if occurred would imply that the transfer in the presence of lipids should be independent of the lipid concentration. In the presence of a large excess of lipids where all the fluorescent parameters are plateauing, the average distance between fluorophores can be estimated in 21 Å. This value is similar to that for the monomeric α-helical melittin obtained in methanol $R = 20.2$ Å. Then we propose a monomeric state for melittin when bound to lipid membranes even when the peptide is incorporated from the water soluble tetramer (Fig. 7).

The general behaviour of DNC–melittin that we argue in the presence of lipids also can be extrapolated to what occurs in the presence of cell membranes. In such case, a biphasic energy transfer curve also indicates maximal peptide–peptide interactions at $R_i = 50$ which decreases at higher R_i values. In such conditions, we do not detect direct significant contributions from membrane proteins, and our fluorescence data are better accounted for peptides surrounded by negatively charged lipids.

In conclusion, the results of the present study suggest that the initial interaction between melittin and the red blood cells could be merely electrostatic through the basic C-terminus but the peptide is not fully stabilised at the membrane plane and it remains in a low α-helical conformation. The next step after electrostatic interaction would be a peptide stabilisation in the membrane. Thus, conformational changes are induced to yield a peptide–lipid complex having the lowest possible energy state. Our results suggest that this complex is formed by monomeric highly α-helical melittin and predominantly negatively charged phospholipids. Nevertheless, we could not observe the presence of integral membrane proteins close enough to allow energy transfer between their intrinsic tryptophan residues and the dansyl group at the C-terminus of DNC–melittin, although at present we cannot rule out the possibility of some other kind of peptide–protein interaction at larger distances. Then, the insertion of the toxin in the bilayer will induce a re-organisation of the membrane components that facilitates the haemoglobin release and the concomitant cell collapse. After the lysis has been completed, our data suggest that melittin is complexed with phospholipids mainly negatively charged.

Although DNC–melittin enlightens our knowledge in the behaviour of the toxin in the presence of natural membranes, it still remains to more definitively settle the parallelism between the perturbation induced by melittin on lipids and on cell membranes, i.e., what is the detailed structure of the ‘soluble’ complexes here detected and to which extent are they involved in the mechanism of action of cytolytic toxins.

Acknowledgements

We thank Dr. J.C. Talbot for his help and criticism on anisotropy and RET measurements. This work was supported by grant No. PB93-0359 from DGICYT.

References

[1] Y. Goto, Y. Hagihara, Biochemistry 31 (1992) 732–738.
[2] E. Pérez-Payá, R.A. Houghten, S.E. Blondelle, J. Biol. Chem. 270 (1995) 1048–1056.
[3] J.C. Talbot, J. Dufourcq, J. Bony, J.F. Faucon, C. Lussan, FEBS Lett. 102 (1979) 191–193.
[4] W. Wilcox, D. Eisenberg, Protein Sci. 1 (1992) 641–653.
[5] T.C. Terwilliger, D. Eisenberg, J. Biol. Chem. 257 (1982) 6010–6015.
[6] T.C. Terwilliger, D. Eisenberg, J. Biol. Chem. 257 (1982) 6016–6022.
[7] C.E. Dempsey, Biochim. Biophys. Acta 1031 (1990) 143–161.
[8] A. Hermetter, J.R. Lakowicz, J. Biol. Chem. 261 (1986) 8243–8248.
[9] E. John, F. Jähnig, Biophys. J. 60 (1991) 319–328.
[10] G. Schwarz, G. Beschiaschvili, Biochim. Biophys. Acta 979 (1989) 82–90.
[11] J.C. Talbot, J.F. Faucon, J. Dufourcq, Eur. Biophys. J. 15 (1987) 147–157.
[12] H. Vogel, F. Jähnig, Biophys. J. 50 (1986) 573–582.
[13] C. Altenbach, W.L. Hubbell, Proteins: Struc. Func. Genetics 3 (1988) 230–242.
[14] M.J. Clague, R.J. Cherry, Biochim. Biophys. Acta 980 (1989) 93–100.
[15] M.J. Dufton, R.C. Hider, R.J. Cherry, Eur. Biophys. J. 11 (1984) 17–24.
[16] M. van Veen, R.J. Cherry, FEMS Microb. Immunol. 105 (1996) 147–150.

[17] M.T. Tosteson, S.J. Holmes, M. Razin, D.C. Tosteson, J. Membr. Biol. 87 (1985) 35–44.
[18] T. Katsu, C. Ninomiya, M. Kuroko, H. Kobayashi, T. Hirota, Y. Fujita, Biochim. Biophys. Acta 939 (1988) 57–63.
[19] T. Katsu, M. Kuroko, T. Morikawa, K. Sanchica, Y. Fujita, H. Yamamura, M. Uda, Biochim. Biophys. Acta 983 (1989) 135–141.
[20] J. Dufourcq, J.F. Faucon, G. Fourche, J.L. Dasseux, M. LeMaire, T. Gulik- Krzywicki, Biochim. Biophys. Acta 859 (1986) 33–48.
[21] E. Pérez-Payá, L. Braco, C. Abad, J. Dufourcq, J. Chromatogr. 548 (1991) 351–359.
[22] E. Pérez-Payá, E. Thiaudiere, C. Abad, J. Dufourcq, FEBS Lett. 278 (1991) 51–54.
[23] S. Nury, J.C. Meunier, A. Mouranche, Eur. J. Biochem. 180 (1989) 161–166.
[24] A.J. Weaver, M.D. Kemple, F.G. Prendergast, Biochemistry 28 (1989) 8614–8623.
[25] D.J. Hanahan, J.E. Ekholm, Meth. Enzymol. 31 (1974) 168–180.
[26] C.C. Sweeley, G. Dawson, In: E. Jamieson, D. Greenwalt (Eds.), Red-Cell Membrane, Structure and Function, Lippincott, Philadelphia, 1969, pp. 172–227.
[27] C.C. Condie, S.C. Quay, J. Biol. Chem. 258 (1983) 8231–8234.
[28] L. Lorand, L.K. Campbell, Anal. Biochem. 44 (1971) 207–220.
[29] L. Stryer, Annu. Rev. Biochem. 47 (1978) 819–846.
[30] J.R. Lakowicz, I. Gryczynski, W. Wiczk, G. Laczko, F.C. Prendergast, M.L. Johnson, Biophys. Chem. 36 (1990) 99–115.
[31] C. Wolff, C. Lai, Arch. Biochem. Biophys. 268 (1989) 536–545.
[32] J.F. Faucon, J. Dufourcq, C. Lussan, FEBS Lett. 102 (1979) 187–190.
[33] A.M. Batenburg, J.C.L. Hibbeln, B. de Kruijff, Biochim. Biophys. Acta 903 (1987) 155–165.
[34] S. Ohki, E. Marcus, D.K. Sukumaran, K. Arnold, Biochim. Biophys. Acta 1194 (1994) 223–232.
[35] M. Langner, S.W. Hui, Chem. Phys. Lipids 60 (1991) 127–132.
[36] S.E. Blondelle, R.A. Houghten, Peptide Res. 4 (1991) 12–18.
[37] S.E. Blondelle, R.A. Houghten, Biochemistry 30 (1991) 4671–4678.
[38] S.E. Blondelle, L.R. Simpkins, E. Pérez-Payá, R.A. Houghten, Biochim. Biophys. Acta 1202 (1993) 331–336.
[39] W.F. DeGrado, G.F. Musso, M. Lieber, E.T. Kaiser, F.J. Kézdy, Biophys. J. 37 (1982) 329–338.
[40] P. Schoch, D.F. Sargent, Biochim. Biophys. Acta 602 (1980) 234–247.
[41] J. Dufourcq, F. Faucon, Biochim. Biophys. Acta 467 (1977) 1–11.
[42] I. Cornut, B. Desbat, J.M. Turlet, J. Dufourcq, Biophys. J. 70 (1996) 305–312.
[43] S.F. Sui, H. Wu, Y. Guo, K.S. Chen, J. Biochem. 116 (1994) 482–487.
[44] I. Cornut, J.L. Büttner, J.L. Dasseux, J. Dufourcq, FEBS Lett. 349 (1994) 29–33.
[45] R.M. Epand, B.T.C. Leon, Biochemistry 31 (1992) 1150–1554.